

Gate-Tunable Superconducting-Insulating Transition in Tin-Decorated Graphene

Adrien Allain,¹ Zheng Han,¹ and Vincent Bouchiat¹

¹*Institut Néel, CNRS-UJF-INP, BP 166, 38042 Grenoble cedex 9, France.*

(Dated: 11 août 2022)

The discovery of the superconductor-insulator transition (SIT) in thin films has spawned a considerable amount of work over the past thirty years [1]. This quantum phase transition [2] is relevant to understand the interplay between superconductivity and localization [3] and to probe the mechanisms of high-temperature superconductivity [4, 5]. However, the nature of the insulating phase [6], together with the origin of the intervening metallic region [7] and the giant positive magnetoresistance [8] are still open questions. Here we report an electrostatically-controlled SIT in graphene decorated by tin nanoparticles. This hybrid superconductor exhibits features related to granular superconductivity, a giant magnetoresistance peak, as well as an intermediate metallic behavior. It allows crossing the transition by adjusting the carrier density under constant disorder and sheds light on the emergence of superconductivity through percolation in granular systems. Finally it demonstrates the potential of graphene as a versatile substrate for the realization of hybrid structures.

Graphene is an easily gate-tunable two dimensional electron gas (2DEG) [9]. Its surface is exposed to the environment and accessible for non-covalent functionalization, making it a very appealing starting material for a variety of applications such as sensing or spintronics applications. Even though no intrinsic superconductivity has yet been experimentally shown, it can carry supercurrent by proximity effect [10], which is expected to exhibit exotic properties due to the specular Andreev reflection of Dirac fermions [11]. In the present study, the proximity effect is not generated from the superconducting contacts, but by coupling graphene's surface to a 2D network of superconducting particles [12], with graphene mediating superconductivity on a macroscopic scale. Previous experiments using exfoliated graphene have shown [13] that such a hybrid system can exhibit a gate-tunable Berezinsky-Kosterlitz-Thouless (BKT) transition towards a fully bidimensional superconducting state with a critical temperature related to the normal state resistivity. In that experiment, the mean free path and the superconducting coherence length exceeded the average gap width separating neighboring tin nanoparticles, resulting in homogeneous 2D superconductivity. Here, the main and crucial difference is the use of millimeter-scale graphene layers grown by chemical va-

pour deposition (CVD) instead of micron-scaled exfoliated graphene. Our CVD samples have a significant electronic disorder which induces strong electron localization under 1K (see Supplementary Figure S2 and S4 and Supplementary Table S1).

We fabricated samples by connecting graphene flakes transferred on oxidized silicon [14] (see Methods). A nominal thickness of 10 nm of tin was evaporated on the whole sample by thermal evaporation. Tin's dewetting produces a self-assembled, non-percolating array of pancake-like nanoparticles [13] (see inset of Fig.1a and Supplementary Figure S1). The typical lateral size of a tin island is 80 nm, with a 13 nm gap in-between islands.

Samples have shown two kinds of behavior depending on their room temperature resistivity. The low resistivity devices (typically ≤ 10 k Ω/\square) showed superconductivity for all gate voltages with a variable transition temperature, similarly to what was reported for exfoliated samples [13]. Here, we will focus on the other type of devices, which exhibited a high sheet resistance (≥ 15 k Ω/\square) at room temperature.

Upon cooling from room temperature down to 6K, the resistivity increase ranges from 20% up to 100% at the charge neutrality point. This behaviour is consistent with the enhanced weak localization and electron-electron interactions expected in 2D metals [15]. Just above the critical temperature of bulk tin ($T_c^{Sn} = 3.7$ K, black dotted line in Fig.1a), a 10% resistance drop is observed (see Fig.1b), arising from superconducting fluctuations in graphene near the tin islands. Then a broad transition takes place, either towards a superconducting state at high electrostatic doping (for a voltage offset from the charge neutrality point $\Delta V > 45$ V), or towards an insulating state for voltages closer to the charge neutrality point ($\Delta V < 10$ V). In between these two gate voltages, the resistivity levels off at low temperatures (inset of Fig.1), suggesting an intermediate metallic behaviour. On the superconducting side, the system follows an "inverse Arrhenius law" $R \propto R_0 \exp\left(\frac{T}{T_0}\right)$, as already reported in quench condensed granular films [16]. It differs from the case of clean graphene [13], for which a BKT superconducting transition was observed for all gate voltages. Significant fluctuations and leveling in the region just before superconductivity sets in (see Fig.2, bump near +10 V) are indicative of a percolative behaviour. The amplitude of the critical current also supports this picture, as it was repetitively measured to be on the order

of 1 μA , which corresponds to a critical current density of 5.10^{-4} A/m, a value 2,000 times smaller than the value found in samples made from exfoliated graphene [13].

Near the charge neutrality point, the resistivity behaves qualitatively the same above 2K. It then reaches a minimum at a gate-dependent temperature (red dotted line in Fig.1b), below which it starts to increase sharply. This re-entrant behaviour is reminiscent of what was observed in granular superconductors [17] or in Josephson junctions arrays [18]. Our system is indeed similar to a granular superconductor in which the role of the intergranular media is taken up by graphene. In such systems, the SIT is driven by the competition between the charging energy E_C of a superconducting island and the Josephson energy $E_J = \frac{1}{2} \frac{\hbar}{4e^2} \frac{\Delta}{R_N} \tanh\left(\frac{\Delta}{2k_B T}\right)$, where R_N is the normal state resistivity of the junction. Dissipative degrees of freedom, such as quasiparticles [20] or capacitive coupling to a 2DEG [21, 22] like graphene [23], lead to renormalization of the charging energy. Here, the leveling of resistivity in the intermediate 'metallic' regime (inset of Fig.1) is indicative of such dissipative processes [19]. Dissipation strength scales as R_N^{-1} , and R_N in turn depends on gate voltage and temperature, as can be seen by applying a magnetic field above the critical field (see Supplementary Figure S3). R_N thus tunes both energies (E_J and E_C) simultaneously, unlike previously considered situations [21–23]. Despite this complex dependence, the phase diagram of the SIT (Fig. 3) shows that the boundary of the insulating region (red dotted line in Fig.1b) can be related to a constant value of R_N .

Plotting the same data as a function of gate (Fig.2), one sees a crossing point at $\cong -20$ V where the resistivity is about $\frac{\hbar}{4e^2}$. This strongly indicates a bosonic quantum phase transition [33]. Around this transition, the resistance varies by more than 7 orders of magnitude over a gate range of 40 V (corresponding to a carrier density change of 3×10^{12} cm^{-2}). This electrostatically driven transition shows a strongly insulating state, with exponential divergence of the resistivity.

The magnetoresistance curves in the insulating and superconducting region are presented in Fig.4a. Such a non-monotonous behaviour has been widely reported in superconducting thin films. By gating the sample, we observed a continuous crossover between different magnetoresistance regimes [24]. In the superconducting state (red curve in Fig.4), the small resistance overshoot at intermediate magnetic field can be understood in terms of Galitski-Larkin correction to the conductivity [25]. The inflection point corresponds to the critical field expected in tin nanoparticles [26]. However, the behaviour in the insulating region (black curve in Fig.4a) cannot be explained with perturbation theory. Here, the resistance at intermediate field ($B = 0.15$ T) is about 40 times higher than the resistance in the normal state ($B = 1$ T). Such huge effects have been reported in amorphous thin

films [27–29], and have been explained [30] to stem from the underlying nature of superconductivity in amorphous thin films, which is inhomogeneous [31, 32] near the transition. In a granular system, since grains of different sizes have different critical fields, there exists an intermediate field where half of the grains are superconducting (S) and the other half are normal (N). N-S junctions can prevent percolation as they provide barriers for both quasiparticles and Cooper pairs. As we move away from the insulating region (by increasing ΔV), the resistivity maximum is shifted towards higher magnetic field. This indicates that islands with the smaller critical fields ($B_C \approx 0.15$ T) play a crucial role in the percolation process, whereas deep in the superconducting region, coupling is established directly between other islands.

Finally, the temperature dependance of the system when biased at $\Delta V = 0$ and for $B = 0.15$ T (i.e. in the region where Cooper pairs are localized) does not quite follow the activation law predicted by Beloborodov *et al.* [30]. Instead it shows an Efros-Schklovsky like behaviour $T \propto \exp\left(\frac{T_1}{T}\right)^{\frac{1}{2}}$ with an activation energy $T_1' = 32.6$ K (see Fig.4b), suggesting that Coulomb interactions may play an important role in the transport.

Going back to the gate-induced SIT, Fig.5 shows how the data can be interpreted as a quantum phase transition, using finite-size scaling [33]. The voltage range around the critical gate voltage $V_{Gc} = -20$ V was chosen the largest possible ($\pm 6V$) while still retaining a universal exponent on both (insulating and superconducting) sides. The temperature range was chosen to lie above the metallic region, as suggested previously [19]. Interestingly, despite the presence of dissipation, the critical resistance lies very close to the "universal" value : $\frac{R_C}{R_Q} \cong 1.2$, $R_Q = \frac{\hbar}{4e^2}$. This may be an indication that we are in the regime of low dissipation, where the dynamical critical exponent z is still equal to 1 [34]. The exponent $z\nu$ has been evaluated using the two methods described in [35]. The first method is to multiply each curve by the factor t yielding the best collapse to the first curve, then fitting t to $T^{-z\nu}$. The second method is to take the slope of $\log\left[\left(\frac{\partial R}{\partial V_g}\right)_{V_{g_c}}\right]$ vs $\log(T^{-1})$. The first method (shown in Fig.5) leads to $z\nu = 1.05 \pm 0.10$ while the second method gives a value of $z\nu = 1.18 \pm 0.02$ (see Supplementary Figure S5). The second method is probably more accurate, as it is assured to lie within the critical region. This value is close to other reported values of $z\nu$ in thickness-tuned transition in Bi [35]. It is in good agreement with recent theoretical developments on the superfluid transition in disordered two-dimensional granular systems [36].

Unlike previously reported gate-induced SITs which either showed a partial SIT transition towards a weakly localized metal [4, 37, 38] or involved ionic gating, which freezes at low temperatures [5], the SIT transition can

be gated continuously at low temperatures leading to a very strong transconductance (Fig.2), which could have application like transition-edge detector. The recently demonstrated metal-insulator transition in ultra-clean graphene samples [39] also opens exciting new perspectives to probe the SIT in the opposite limit of very low disorder. The present experiment paves the way to the realization of more complex graphene-based hybrid materials where graphene acts as a tunable medium or adjustable environment that controls the establishment of long-range electronic orders, such as superconductivity or ferromagnetism.

METHODS

Sample Preparation

Graphene is grown using a chemical vapor deposition (CVD) technique on copper foils (typically 25 μm thick, from Alfa-Aesar) following the methods described in [14]. During the growth, a flow of methane (CH_4) provides the carbon feedstock, while forming gas (H_2/Ar 1:8) limits the reaction and only single or few layers of graphene are obtained. After growth, the graphene is protected with a support layer of 1 μm -thick polymethylmethacrylate (PMMA), and copper is etched away using a solution of 0.2 g/ml sodium persulfate ($\text{Na}_2\text{S}_2\text{O}_8$). The graphene remains attached to PMMA and floats in the solution. It is then carefully transferred onto a wafer of degenerately doped oxidized silicon and PMMA is removed using acetone wash followed by thermal annealing at 380°C/1h under Argon atmosphere. Tin is deposited on the whole sample using room temperature Joule evaporation. Pd/Au electrodes are subsequently deposited using a millimeter scaled metal foil stencil mask in a four-probe geometry aligned on top of the graphene sheet. Supplementary Figure S1 shows a typical sample after fabrication. The fabricated samples were about 5 mm in length and 3 mm in width, sizes that could not previously be obtained using exfoliated graphene. Such a macroscopic sample allowed mesoscopic effects such as universal conductance fluctuations to be averaged out, which is crucial when studying how the phase transition scales.

Several samples were measured, and the number of graphene layers was varied (from 1 to 3), as well as the thickness of tin (8-20 nm). However, we did not see a direct correlation between these parameters and the behavior of the device. We could only relate it to the normal state resistivity of graphene. Only graphene showing a high resistivity at room temperature (>15 k Ω) would behave as an insulator below the tin's superconducting transition temperature (3.7 K). The other samples behaved like the ones studied by Kessler et al. [13], showing much higher

critical current density and a gate-tunable Berezinsky-Kozterlitz-Thouless transition.

Measurement setup

The sample was thermally anchored to the mixing chamber of a He3/He4 dilution cryostat and connected to highly filtered measurement lines. The setup allowed the temperature to be continuously varied between 10 K and 0.03K. The differential resistance was recorded using a lock-in amplifier operated in a four-probe configuration at frequencies between 9 Hz and 37 Hz, with an excitation current of 1 nA. In the high impedance state, a two-probe, voltage-biased configuration was used using an electrometer or a current-to-voltage converter to record the current.

-
- [1] Gantmakher, V.F. & Dolgoplov, V.T. Superconductor-insulator quantum phase transition. *Physics Uspekhi* **53**, 1 (2010).
 - [2] Sondhi, S.L., Girvin, S.M., Carini, J.P. & Shahar, D. Continuous quantum phase transitions. *Rev. Mod. Phys.* **69**, 315 (1997).
 - [3] Goldman, A.M. & Markovic, N. Superconductor-insulator transitions in the two-dimensional limit. *Phys. Today* **51**, No. 11, 39 (1998).
 - [4] Bollinger, A.T. *et al.* Superconductor-insulator transition in $\text{La}_{2-x}\text{Sr}_x\text{CuO}_4$ at the pair quantum resistance. *Nature* **472**, 458 (2011).
 - [5] Leng, X., Garcia-Barriocanal, J., Bose, S., Lee, Y. & Goldman, A.M. Electrostatic control of the evolution from a superconducting phase to an insulating phase in ultrathin $\text{YBa}_2\text{Cu}_3\text{O}_{7-x}$ films. *Phys. Rev. Lett.* **107**, 027001 (2011).
 - [6] Fisher, M.P.A., Weichman, P.B., Grinstein, G. & Fisher, D.S. Boson localization and the superfluid-insulator transition. *Phys. Rev. B* **40**, 546 (1989).
 - [7] Philips, P. & Dalidovich, D. The elusive Bose metal. *Science* **302**, 243 (2003).
 - [8] Galitski, V.M., Refael, G., Fisher, M.P.A. & Senthil, T. Vortices and quasiparticles near the superconductor-insulator transition in thin films. *Phys. Rev. Lett.* **95**, 077002 (2005).
 - [9] Geim, A.K. & Novoselov, K.S. The rise of graphene. *Nature Mat.* **6**, 183 (2007).
 - [10] Heersche, H.B., Jarillo-Herrero, P., Oostinga, J.B., Vandersypen, L. & Morpurgo, A.F. Bipolar supercurrent in graphene. *Nature* **446**, 56 (2007).
 - [11] Beenakker, C.W.J. Specular Andreev reflection in graphene. *Phys. Rev. Lett.* **97**, 067007 (2006).
 - [12] Feigel'man, M.V., Skvortsov, M.A. & Tikhonov, K.S. Proximity-induced superconductivity in graphene. *JEPT Lett.* **88**, 747 (2008).
 - [13] Kessler, B.M., Girit, C.Ö., Zettl, A. & Bouchiat, V. Tunable superconducting phase transition in metal-decorated graphene sheets. *Phys. Rev. Lett.* **104**, 047001 (2010).

- [14] Li, X.S. *et al.*, Large-area synthesis of high-quality and uniform graphene films on copper foils. *Science* **324**, 1312 (2009).
- [15] Akkermans, E. & Montambaux, G. *Mesoscopic physics of electrons and photons* (Cambridge University Press, 2007).
- [16] Frydman, A., Naaman, O. & Dynes, R.C., Universal transport in two-dimensional granular superconductors. *Phys. Rev. B* **66**, 052509 (2002).
- [17] Jaeger, H.M., Haviland, D.B., Orr, B.G. & Goldman, A.M. Onset of superconductivity in ultrathin granular metal films. *Phys. Rev. B* **40**, 182 (1989).
- [18] van der Zant, H.S.J., Elion, W.J., Geerlings, L.J. & Mooij, J.E., Quantum phase transitions in two dimensions: experiments in Josephson-junction arrays. *et al.*, *Phys. Rev. B* **54**, 10081 (1996).
- [19] Mason, N. & Kapitulnik, A., Dissipation effects on the superconductor-insulator transition in 2D superconductors. *Phys. Rev. Lett.* **82**, 5341 (1999).
- [20] Chakravarty, S., Kivelson, S., Zimanyi, G.T. & Halperin, B.I., Effect of quasiparticle tunneling on quantum-phase fluctuations and the onset of superconductivity in granular films. *Phys. Rev. B* **35**, 7256 (1987).
- [21] Rimborg, A.J. *et al.*, Dissipation-driven superconductor-insulator transition in a two-dimensional Josephson-junction array. *Phys. Rev. Lett.* **78**, 2632 (1997).
- [22] Wagenblast, K.-H., van Otterlo, A., Schön, G. & Zimanyi, G.T., Superconductor-insulator transition in a tunable dissipative environment. *Phys. Rev. Lett.* **79**, 2730 (1997).
- [23] Lutchyn, R.M., Galitski, V., Refael, G. & Das Sarma, S. Dissipation-driven quantum phase transition in superconductor-graphene systems. *Phys. Rev. Lett.* **101**, 106402 (2008).
- [24] Steiner, M.A., Boebinger, G. & Kapitulnik, A., Possible field-tuned superconductor-insulator transition in high-Tc superconductors: implications for pairing at high magnetic fields. *Phys. Rev. Lett.* **94**, 107008 (2005).
- [25] Galitski, V.M. & Larkin, A.I., Superconducting fluctuations at low temperature. *Phys. Rev. B* **63**, 174506 (2001).
- [26] Wang, X-L., Feyngenson, M., Aronson, M.C. & Han, W.-Q., Sn/SnOx core-shell nanospheres: synthesis, anode performance in Li-Ion batteries, and superconductivity. *J. Phys. Chem. C* **114**, 14697 (2010).
- [27] Sambandamurthy, G., Engel, L.W., Johansson, A. & Shahr, D., Superconductivity-related insulating behavior. *Phys. Rev. Lett.* **92**, 107005 (2004).
- [28] Nguyen, H.Q., *et al.*, Observation of giant positive magnetoresistance in a Cooper pair insulator. *Phys. Rev. Lett.* **103**, 157001 (2009).
- [29] Baturina, T.I. , Mironov, A.Yu., Vinokur, V.M., Baklanov, M.R. & Strunk, C., Localized superconductivity in the quantum-critical region of the disorder-driven superconductor-insulator transition in TiN thin films. *Phys. Rev. Lett.* **99**, 257003 (2007).
- [30] Beloborodov, I.S., Fominov, Ya.V., Lopatin, A.V. & Vinokur, V.M., Insulating state of granular superconductors in a strong-coupling regime. *Phys. Rev. B* **74**, 014502 (2006).
- [31] Sacépé, B. *et al.* Disorder-induced inhomogeneities of the superconducting state close to the superconductor-insulator transition. *Phys. Rev. Lett.* **101**, 157006 (2008).
- [32] Sacépé, B. *et al.*, Localization of preformed Cooper pairs in disordered superconductors. *Nature Phys.* **7**, 239 (2011).
- [33] Fisher, M.P.A., Grinstein, G. & Girvin, S.M. Presence of quantum diffusion in two dimensions: Universal resistance at the superconductor-insulator transition. *Phys. Rev. Lett.* **64**, 587 (1990).
- [34] Wagenblast, K.-H., van Otterlo, A., Schön, G. & Zimanyi, G.T., New universality class at the superconductor-insulator transition. *Phys. Rev. Lett.* **78**, 1779 (1997).
- [35] Markovic, N., Christiansen, C., mack, A.M., Huber, W.H. & Goldman, A.M., Superconductor-insulator transition in two dimensions. *Phys. Rev. B* **60**, 4320 (1999).
- [36] Iyer, S., Pekker, D. & Refael, G. A Mott glass to superfluid transition for random bosons in two dimensions. *arXiv* 1110:3338v1 (2011).
- [37] Parendo, K.A. *et al.* Electrostatic tuning of the superconductor-insulator transition in two dimensions. *Phys. Rev. Lett.* **94**, 197004 (2005).
- [38] Caviglia, A.D. *et al.* Electric field control of the LaAlO3/SrTiO3 interface ground state. *Nature* **456**, 624 (2008).
- [39] Ponomarenko, A.L. *et al.* Tunable metal-insulator transition in double-layer graphene heterostructure. *Nature Phys.*, in Press, doi:10.1038/nphys2114 (2011).

ACKNOWLEDGEMENTS

This work is partially supported by ANR-BLANC SuperGraph, ERC Advanced Grant MolNanoSpin No. 226558 and the Nanosciences Foundation of Grenoble. Samples were fabricated in the NANOFAB facility of the Néel Institute. We acknowledge support and stimulating discussions from H. Arjmandi-Tash, N. Bendiab, J. Coraux, L. Marty, B. Sacépé and W. Wernsdorfer from Neel Institute, Ç.Ö. Girit, B.M. Kessler and A. Zettl from U.C. Berkeley and M.V. Feigel'man from L.D. Landau Institute.

AUTHOR CONTRIBUTIONS

V.B. and A.A. conceived the experiments, Z.H. grew the graphene, A.A. and Z.H. fabricated the samples and carried out the measurements, A.A. and V.B. analyzed the data and wrote the main paper and supplementary informations.

COMPETING FINANCIAL INTERESTS

The authors declare no competing financial interests.

FIGURES

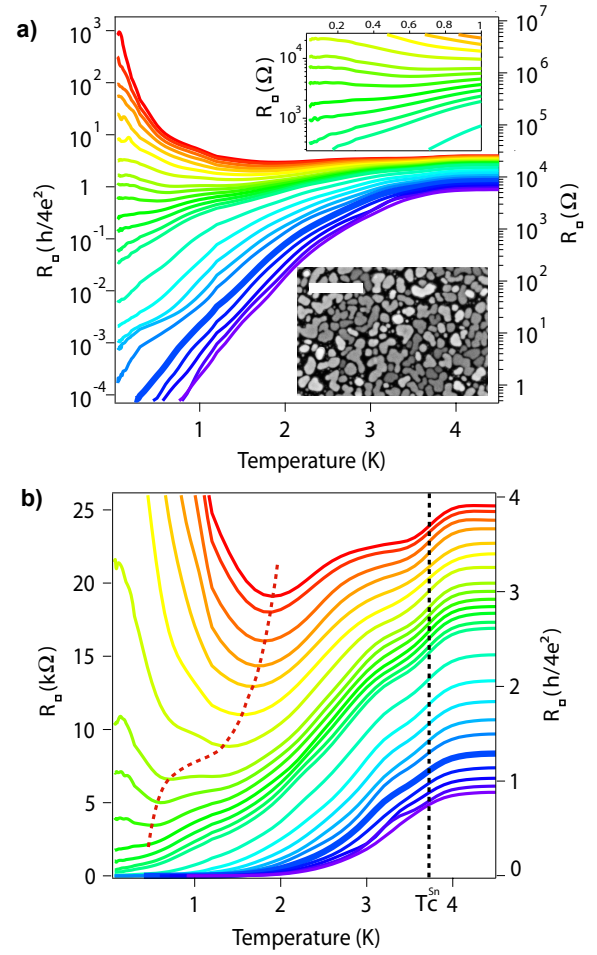


FIGURE 1. **Resistivity as a function of temperature for different gate voltages.** Resistivity as a function of sample temperature for different gate voltages. From top to bottom, voltage offsets from the charge neutrality point ($V_D = -36$ V, see Fig.2) are $\Delta V = Vg - V_D = 0, 3, 6, 8, 10, 12, 14, 16, 17, 18, 19, 20, 21, 22, 26, 31, 36, 41, 46, 56, 66, 76, 86, 96$ V. **a** : Resistivity plotted on a log scale. Upper inset : zoom of the critical region. Lower inset : SEM picture of the device showing tin islands. The scale bar is 300 nm wide. **b** : Same data (lower part) plotted on a linear scale to emphasize the behaviour between 1 K and 4 K. The black dashed line indicates the critical temperature of tin. The red dashed line is a guide to the eye showing the minimum resistivity.

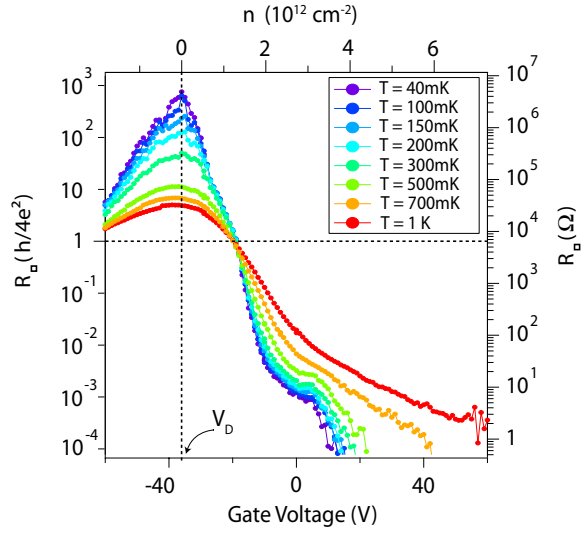


FIGURE 2. **Resistivity as a function of gate voltage for different temperatures.** Gate voltage dependence of resistivity for the lowest temperatures. The vertical dotted line indicated the charge neutrality point. The horizontal one indicated the quantum of resistance for Cooper pairs $R_Q = \frac{h}{4e^2}$ (Top axis : carrier density calculated using the surfacic gate capacitance for 285 nm of SiO₂ $C_{bg} = 121 \mu\text{F}/\text{m}^2$).

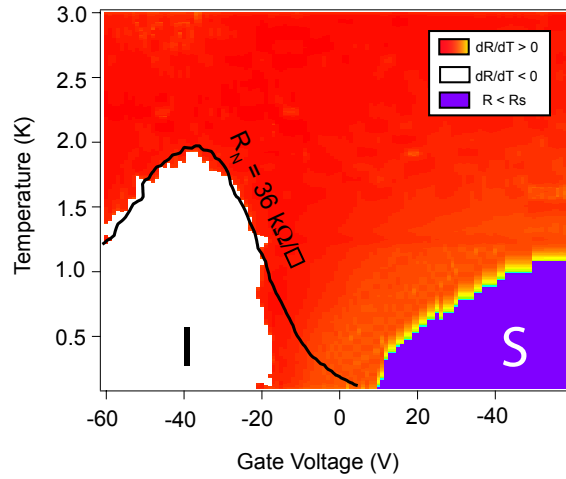


FIGURE 3. **Phase diagram extracted from temperature data.** $\log\left(\frac{\partial R}{\partial T}\right)$ vs gate voltage and temperature. I stands for "Insulating", and S for "Superconducting". We call superconducting the region where R is below the noise floor ($R_S = 2\Omega$). The black line is an iso-value of the normal state resistivity obtained at $B = 1 \text{ T}$ (see Supplementary Figure S3).

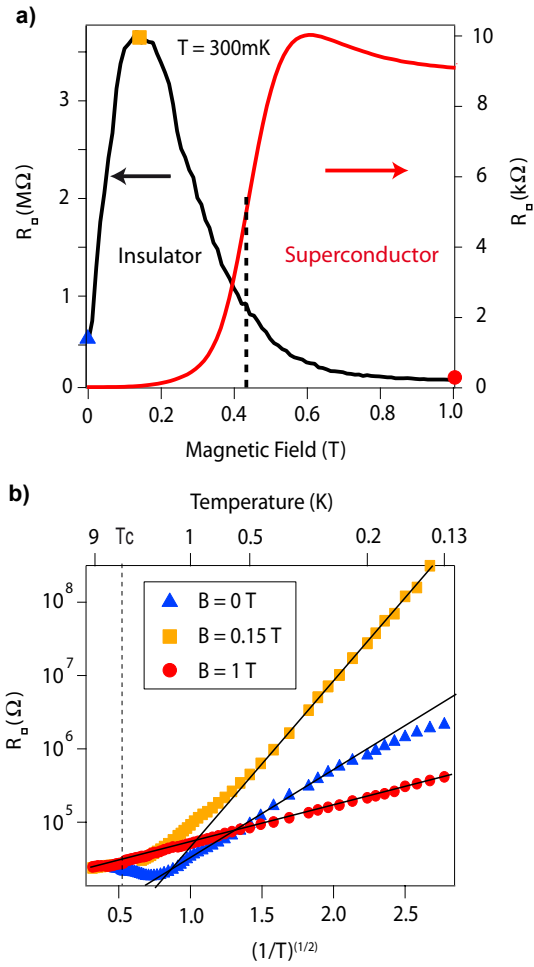


FIGURE 4. **Effect of magnetic field.** **a** : Resistivity as a function of magnetic field, measured at $T = 300 \text{ mK}$. Black curve shows the magnetoresistance at the charge neutrality point. The red curve has been measured deep in the superconducting region. **b** : Temperature dependence of the resistivity at three different magnetic fields (indicated in the upper panel). The black lines are fits to the Efros-Schklovsky law, giving the following activation temperatures : $T_1 = 7.8 \text{ K}$, $T_1' = 32.6 \text{ K}$, and $T_1'' = 2.5 \text{ K}$ for $B = 0 \text{ T}$, 0.15 T and 1 T , respectively.

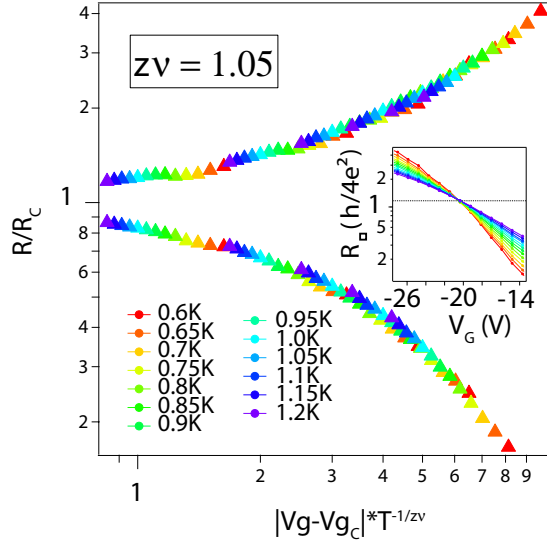


FIGURE 5. **Scaling analysis.** Finite-size scaling analysis of the quantum phase transition, using data of Fig.2. The best collapse was found using $\nu z = 1.05 \pm 0.05$. Inset : subset of the data used for the scaling : $0.6 \text{ K} < T < 1.3 \text{ K}$ and a gate voltage interval of $\pm 6 \text{ V}$ around the critical point $V_{Gc} = -20 \text{ V}$.